

Sailfish Optimizer with EfficientNet Model for Apple Leaf Disease Detection

Mazen Mushabab Alqahtani¹, Ashit Kumar Dutta², Sultan Almotairi³, M. Ilayaraja⁴,
Amani Abdulrahman Albraikan⁵, Fahd N. Al-Wesabi^{6,7,*} and Mesfer Al Duhayyim⁸

¹Physical Therapy Department, Majmaah University, Majmaah, 11952, Saudi Arabia

²Department of Computer Science and Information Systems, College of Applied Sciences, AlMaarefa University, Ad Diriyah, 13713, Riyadh, Saudi Arabia

³Department of Natural and Applied Sciences, Faculty of Community College, Majmaah University, Majmaah, 11952, Saudi Arabia

⁴School of Computing, Kalasalingam Academy of Research and Education, Krishnankoil, 626128, India

⁵Department of Computer Sciences, College of Computer and Information Sciences, Princess Nourah bint Abdulrahman University, P.O.Box 84428, Riyadh, 11671, Saudi Arabia

⁶Department of Computer Science, College of Science & Art at Mahayil, King Khalid University, 62529, Saudi Arabia

⁷Faculty of Computer and IT, Sana'a University, Sana'a, 1247, Yemen

⁸Department of Natural and Applied Sciences, College of Community - Aflaj, Prince Sattam Bin Abdulaziz University, Saudi Arabia

*Corresponding Author: Fahd N. Al-Wesabi. Email: falwesabi@kku.edu.sa

Received: 18 November 2021; Accepted: 17 January 2022

Abstract: Recent developments in digital cameras and electronic gadgets coupled with Machine Learning (ML) and Deep Learning (DL)-based automated apple leaf disease detection models are commonly employed as reasonable alternatives to traditional visual inspection models. In this background, the current paper devises an Effective Sailfish Optimizer with EfficientNet-based Apple Leaf disease detection (ESFO-EALD) model. The goal of the proposed ESFO-EALD technique is to identify the occurrence of plant leaf diseases automatically. In this scenario, Median Filtering (MF) approach is utilized to boost the quality of apple plant leaf images. Moreover, SFO with Kapur's entropy-based segmentation technique is also utilized for the identification of the affected plant region from test image. Furthermore, Adam optimizer with EfficientNet-based feature extraction and Spiking Neural Network (SNN)-based classification are employed to detect and classify the apple plant leaf images. A wide range of simulations was conducted to ensure the effective outcomes of ESFO-EALD technique on benchmark dataset. The results reported the supremacy of the proposed ESFO-EALD approach than the existing approaches.

Keywords: Agriculture; computer vision; image processing; deep learning; metaheuristics; image segmentation



This work is licensed under a Creative Commons Attribution 4.0 International License, which permits unrestricted use, distribution, and reproduction in any medium, provided the original work is properly cited.

1 Introduction

Agriculture is one of the primary sectors that contribute to economic development of a country. Being a backbone of country's development, the sector faces a lot of challenges to survive. Plant disease is one such prominent challenge that causes disruption in agricultural crop production. However, this issue can be resolved through the adoption of advanced agricultural technologies [1]. Having said that, it is really hard to attain the goal, owing to lack of awareness, high cost, implementation challenges, etc. But, the costs incurred upon the technique can be decreased by employing image processing applications that make use of Deep Learning (DL) and Machine Learning (ML) methods. Identification of leaf disease using Artificial Intelligence (AI) technique [2] can result in high yield and uncompromised quality products compared to traditional disease detection techniques. Furthermore, leaf diseases tend to occur based on climate and survival conditions. At most of the times, leaf diseases are caused by fungi, viruses, and bacteria [3]. Apple is one of the most cultivated fruits around the globe and it possess high medicinal and nutritional values. But many diseases recurrently affect apple production on a massive scale which cause considerable economic loss. Hence, effective and timely recognition of apple leaf disease is a critical challenge to overcome for healthy growth of apples and increased production. Recently, it has become a hot research topic in agriculture [4]. There is a considerable increase observed in apple planting region and output in the recent years, thanks to its high nutritional content and economic value. But, apple plant leaf disease incur heavy loss in terms of production and economic activities. It reduces the quantity and quality of fruit industry outputs. Hence, it becomes necessary to have a precise detection method for apple leaf disease [5].

In general, visual inspection by professionals is the preferred method for diagnosing plant diseases for a long time. But it involves the risk for error, because of individual perceptions [6]. In such event, many imaging and spectroscopic methods have been investigated for plant disease detection. But there is a need exists for bulky sensors and precise instruments that produce high efficiency at low cost. With the popularity of digital cameras and electronic gadgets in recent years, automated plant disease detection using ML method is being extensively applied these days as an effective alternative [7]. Over the past few years, conventional ML techniques have made considerable progress in apple leaf diseases detection. DL techniques performed an extraordinary innovation in advanced Computer Vision (CV) systems, owing to the development of deep convolution network in AlexNet [8]. Further, it is also commonly employed in diagnosis and identification of plant disease, thanks to its excellent robustness and automated extraction of image features. Many authors have used DL method in the detection of apple leaf diseases.

In the study conducted by Zhong et al. [9], apple leaf image dataset that consists of 2462 images, belonging to six apple leaf diseases, was employed for method evaluation and data modeling. In this study, DenseNet-121 deep convolutional network, three regression techniques, focus loss function and multilabel classification were presented for the identification of apple leaf disease. Michalak et al. [10] introduced an apple leaf disease recognition technique based on pattern recognition methods and image and processing techniques. In this study, a colour conversion technique for the input Red, Green, and Blue (RGB) image was initially presented. Later RGB pattern was changed to grey, and Hue, Saturation, and Intensity (HSI) patterns. The background was detached according to certain threshold values. Later, the disease spot image was divided using Region Growing Algorithm (RGA). A total of 38 features, used for categorization, such as shape, colour, and texture was extracted from all the spot images. In order to enhance the precision of apple leaf disease diagnosis and decrease the dimensionality of feature space, only the effective features were chosen by integrating Correlation-based Feature Selection (CFS) and Genetic Algorithm (GA) methods. Lastly, the disease was detected using Support Vector Machine (SVM) classification method.

Jiang et al. [11] presented a DL method based on enhanced Convolutional Neural Network (CNN) method for real-time recognition of apple leaf disease. In this study, Apple Leaf Disease Data set (ALDD) was used to validate the proposed model. According to the authors, a novel apple leaf disease recognition method that employs Deep Convolutional Neural Network (DCNN) was presented in this study using Rainbow concatenation and GoogLeNet Inception model. Liu et al. [12] presented a precise detection methodology for apple leaf diseases based on DCNN model. It involves the designing of a new framework using DCNN-based AlexNet and generation of adequate pathological images to identify apple leaf disease. In Umamageswari et al. [13], a novel framework was proposed for the detection of plant leaf diseases. Initially, image contrast level was improved as well as overfitting and unwanted noise were detached. Then, fuzzy c-means based Chameleon Swarm Algorithm (FCM-CSA) was employed for the segmentation of plant leaf disease parts. Next, feature extraction was executed using a fast Grey Level Co-occurrence Matrix (GLCM) feature extraction method. Lastly, Progressive Neural Architecture Search (PNAS) was applied for the identification of plant diseases. Tahir et al. [14] presented a novel deep methodology for the classification of apple leaf diseases. Some of the most popular apple leaf diseases are apple cedar, Apple Scab (AS), and brown spot. After the feature was extracted using Transfer Learning (TL) method, the feature was down-sampled using a new variance-controlled method. Tiwari et al. [15] presented a DL-based method for detection and classification of plant diseases identified from leaf images captured in multiple resolutions. The dense CNN framework was trained on a massive plant leaf image datasets from several nations. The six yields, under 27 distinct classes, were taken in the presented method for both laboratory and on-field conditions into account.

The current research paper devises an Effective Sailfish Optimizer with EfficientNet based Apple Leaf Disease detection (ESFO-EALD) model. The proposed ESFO-EALD technique applies Median Filtering (MF) approach to boost the quality of apple plant leaf images. Moreover, SFO with Kapur's entropy-based segmentation technique is utilized in this study for identification of the affected plant region from test image. Furthermore, Adam optimizer with EfficientNet based feature extraction and Spiking Neural Network (SNN)-based classification are employed for both detection and classification of apple plant leaf images. A wide range of simulations was conducted to validate the effective outcomes of ESFO-EALD technique on benchmark dataset. The results established the supremacy of the proposed ESFO-EALD technique than existing approaches.

Rest of the paper is organized as follows. Section 2 introduces the proposed model, Section 3 validates the proposed model, and Section 4 concludes the work.

2 Materials and Methods

In this study, an effective ESFO-EALD technique has been developed for identification and classification of apple plant leaf images. The proposed ESFO-EALD method involves MF-based pre-processing, SFO using Kapur's entropy-based segmentation, EfficientNet-based feature extraction, Adam optimizer-based hyperparameter tuning, and SNN-based classification. The utilization of ESFO-based threshold value selection and Adam optimizer-based hyperparameter selection help in accomplishing enhanced outcomes. Fig. 1 illustrates the overall process of ESFO-EALD technique.

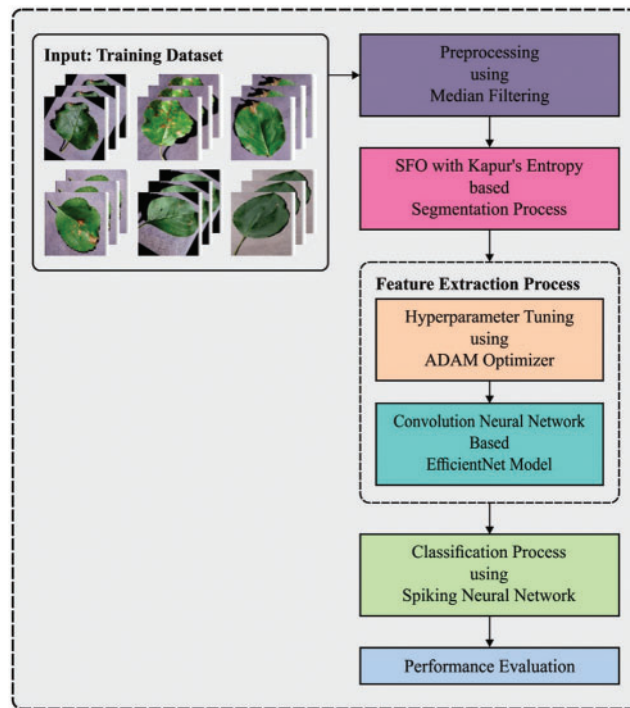


Figure 1: Overall process of ESFO-EALD technique

2.1 Data Collection

In this study, the researchers used benchmark plant disease dataset from Kaggle repository. The dataset includes images under four classes namely AS, Black Rot (BR), Cedar Rust (CR), and healthy (HY). Among these, AS dataset includes 2,016 trained images and 504 tested images. In line with this, BR dataset contains 1,987 trained images and 497 tested images. Moreover, CR dataset comprises of 1,760 trained images and 440 tested images. Furthermore, HY dataset includes 2,008 trained images and 502 tested images.

2.2 MF Based Pre-Processing

Primarily, MF technique gets rid of the noise present in apple plant leaf images. Being a non-linear method, it is effective in decreasing salt-and-pepper or impulsive noises. Further, it also conserves the edges in image effectively, while decreasing random noises. Salt-and pepper or impulsive noise tend to occur due to arbitrary bit error in transmission network. In median filter, the median intensity value of the pixel within the window and a window that slides alongside the image become the output intensity of pixels. Median filtering smoothen the image and is effective in noise reduction. On the contrary to low-pass filter, median filter could retain discontinuity in a step-wise manner and could smoothen some pixels with value that differs considerably from their surroundings without impacting other pixels.

2.3 ESFO with Kapur's Entropy-Based Segmentation

During segmentation, SFO algorithm with Kapur's entropy technique is used to identify the regions affected with plant disease. Kapur's entropy approach is another thresholding method which

is employed in the implementation of segmentation principle. Kapur’s method selects the optimum threshold value-based maximization of entropy. The arithmetical expression is shown in the following equation:

$$F_{kapur}(th) = H_1 + H_2 \tag{1}$$

Here, H_1 and H_2 entropies are calculated as follows.

$$H_1 = \sum_{i=1}^{th} \frac{Ph_i}{\omega_0} \ln \left(\frac{Ph_i}{\omega_0} \right) \text{ and } H_2 = \sum_{i=th+1}^L \frac{Ph_i}{\omega_1} \ln \left(\frac{Ph_i}{\omega_1} \right) \tag{2}$$

Let Ph_i be the probability distribution of intensity levels, $\omega_0(th)$ and $\omega_1(th)$ denote probability distribution-based classes such as C_1 and C_2 . $\ln(\cdot)$ indicates the natural logarithm [16]. Entropy-based model has transformed for multi-threshold values that are analogous to Otsu algorithm. It is significant to divide the image to N classes with $N - 1$ threshold and is expressed through Eq. (3).

$$F_{kapur}(TH) = \sum_{i=1}^N H_i \tag{3}$$

Here, a vector that comprises of numerous thresholds is $TH = [th1, th2, \dots, thN - 1]$. All the entropies are individually calculated with respective values (th), hence Eq. (3). For N , entropy is extended by Eq. (4):

$$H_N^c = \sum_{i=th_{N+1}}^L \frac{Ph_i}{\omega_{N-1}} \ln \left(\frac{Ph_i}{\omega_{N-1}} \right) \tag{4}$$

The probability value occurrence ($\omega_0^c, \omega_1, \dots, \omega_{N-1}$) of N classes and Ph_i denotes the probability distribution. In order to the optimum threshold values of Kapur’s entropy, SFO algorithm is utilized.

SFO is a new, nature-inspired meta-heuristic algorithm which is modelled after a group of hunting sailfish. It demonstrates a remarkable performance compared to commonly available meta-heuristic approaches. The location of i th sailfish in k th searching iteration is represented by $SF_{i,k}$, and its respective fitness is calculated using $f(SF_{i,k})$. Sardine is the other important participant in SFO method. The location of i th sardine is represented by S_i while its respective fitness is evaluated using $f(S_i)$. In SFO model, the sailfish that occupies the optimal location is chosen as ‘elite sailfish’ and it affects the acceleration and maneuverability of sardines during attacks. In addition, the location of an injured sardine, during all the iterations, is chosen as an optimal location for collective hunting by sailfishes. Elite sailfish and the injured sardine are represented as $Y_{elite_{SF}}^i$ and $Y_{injured_S}^i$, correspondingly during i th iteration. At the time of hunting, a sailfish attack alternative method is frequently employed for enhancing the hunting results [17]. The novel location of sailfish $Y_{new_{SF}}^i$ is upgraded by Eq. (5).

$$Y_{new_{SF}}^i = Y_{elite_{SF}}^i - \lambda_i \times \left(random(0, 1) \times \left(\frac{Y_{elite_{SF}}^i - Y_{injured_S}^i}{2} \right) - Y_{current_{SF}}^i \right), \tag{5}$$

Here, $Y_{current_{SF}}^i$ denotes the present location of sailfish and is arbitrarily in the range of zero and one.

The parameter λ_i denotes the coefficient in i th iteration:

$$\lambda_i = 2 \times rand(0, 1) \times SD - SD, \tag{6}$$

Here, SD indicates sardine density that represents the amount of sardines during all the iterations.

The parameter SD is acquired by Eq. (7)

$$SD = 1 - \left(\frac{N_{SF}}{N_{SF} + N_S} \right), \quad (7)$$

In this equation, N_{SF} and N_S signify the amount of sailfish and sardines correspondingly.

During early stage of the hunt, sardines do not get injured/tired and sailfish remain energetic. Sardine can rapidly escape the hunting scene. But, with constant hunting, the strength of sailfish attacks gets reduced gradually. In the meantime, sardines get tired and their awareness about the position of sailfish also gets reduced. As a consequence, the sardine is hunted. According to the algorithmic procedure, the novel location of sardine $Y_{new_S}^i$ gets upgraded by Eq. (8).

$$Y_{new_S}^i = random(0, 1) \times \left(Y_{elite_{SF}}^i - Y_{old_S}^i + ATP \right), \quad (8)$$

Now, $Y_{old_S}^i$ represents the older location of sardine which is in arbitrary range of zero and one. ATP signifies the power of sailfish attack.

The parameter ATP is evaluated using Eq. (9):

$$ATP = B \times (1 - (2 \times Itr \times \varepsilon)) \quad (9)$$

While B and ε represent the coefficients employed for linear reduction of attack power from B to 0 whereas Itr indicates the number of iterations. Since the attack power of sailfish gets reduced over hunting time, this reduction promotes search convergence. Once the attack power (ATP) becomes higher, e.g., greater than 0.5, the location of each sardine also gets upgraded. However, α sardine with β parameter upgrades their locations. The number of sardines that upgrade their location, is measured by Eq. (10):

$$\alpha = N_S \times ATP, \quad (10)$$

Let N_S be the number of sardines during all the iterations. The amount of parameters of the sardine that upgrades its locations is attained as follows.

$$\beta = d_i \times ATP, \quad (11)$$

whereas d_i denotes the number of parameters during i th iteration. Once the sardines are hunted, it is understood that its fitness values should be higher than sailfish. In this condition, the location of sailfish Y_{SF}^i gets upgraded with the newest location of the hunted sardine, Y_S^i to promote the hunting of novel sardines.

$$Y_{SF}^i = Y_S^i \text{ iff } (S_i) < f(SF_i). \quad (12)$$

2.4 Optimal EfficientNet Based Feature Extraction

After segmentation process, the next stage is the generation of useful collection of feature vectors. EfficientNet is a kind of CNN which effectively scales up based on input resolution, layer depth, layer width, and the integration of each factor. It is an advanced DL method that heavily focuses on improving the accuracy and efficiency of the model. It has different versions in the range of B0 to B7. The basic component is MBConv in which the excitation and compression optimization are included. Such block creates shortcuts between the starting and ending points of convolution blocks. The input activation map is extended by 1×1 convolution to increase the depth of feature map. The shortcut connection is utilized in this method to link the narrow layer together, when a wider layer is situated

between the jump links. Fig. 2 illustrates the Efficientnet structure layer [18]. This framework helps in reducing the size and overall amount of essential transactions. Adam optimizer is used to choose the hyperparameters of EfficientNet model proficiently.

Stage	Operator	Resolution	#Channels	#Layers
1	Conv3x3	224 x 224	32	1
2	MBCConv1, k3x3	112 x 112	16	1
3	MBCConv6, k3x3	112 x 112	24	2
4	MBCConv6, k5x5	56 x 56	40	2
5	MBCConv6, k3x3	28 x 28	80	3
6	MBCConv6, k5x5	14 x 14	112	3
7	MBCConv6, k5x5	14 x 14	192	4
8	MBCConv6, k3x3	7 x 7	320	1
9	Conv1x1 and Pooling and FC	7 x 7	1280	1

Figure 2: Layer of efficientnet structure

DL frequently consumes much time and computer resources to train. Thus, optimization techniques are extremely apprehensive. Adam's (adaptive momentum) technique consumes less resources and creates the method convergence earlier. This in turn accelerates the learning speed and enhance the effects. Adam optimizer is a 1st-order optimization approach which changes the conventional stochastic gradient descent procedure. It connects the 2nd moment evaluation on fundamental momentum of 1st-order moment evaluation and increases a moment to Adadelta. The rate of learning for all the parameters gets dynamically modified with the help of 1st and 2nd moment's evaluation of gradients [19]. The bias correction also occurs which further creates the parameters that are comparatively stable.

The iterative equations are as follows:

$$g = (h_{\theta} (x^i - y^i)) x^i,$$

$$m_i = \beta_1 m_{i-1} + (1 - \beta_1) * g,$$

$$v_i = \beta_2 v_{i-1} + (1 - \beta_2) * g^2,$$

$$m_i^{\sim} = \frac{m_i}{1 - \beta_1^i}, \tag{13}$$

$$v_i^{\sim} = \frac{v_i}{1 - \beta_2^i},$$

$$\theta_j = \theta_{j-1} - m_i^{\sim} * \frac{\alpha}{\sqrt{v_i^{\sim} + \epsilon}},$$

where g refers to the computed gradients, m_i stands for 1st moment of gradient g which is also the expectation of gradient g , v_i defines the 2nd moment of gradient g , β_1 implies the 1st-order moment attenuation coefficients, β_2 determines the 2nd moment attenuation coefficients, θ represents the

parameter which requires that resolved (or upgraded), and m_i^{\sim} and v_i^{\sim} denote the offset corrections of m_i and v_i , correspondingly.

2.5 SNN-Based Classification

In this last stage, SNN model is utilized as a classifier to allot proper class labels. SNN method is employed for analyzing the learning process and network dynamic features. Assume that N_i indicates the number of spikes in i th spike train and N_I represents the overall amount of synaptic inputs. w_{io} denotes the synapse weight from i th input to output neurons. t_i^f signifies the f th spike firing time of i input neuron. The neuron possibility can be determined by the summation of potential postsynaptic, which is induced by each input spike from presynaptic neuron. Once the $u(t)$ internal state surpasses the neuron thresholding θ , the output neurons fire at a spike whereas the internal state immediately reduces to resting potentials. This stage is otherwise named as repolarization [20]. The postsynaptic potential neurons at time t can be estimated using the following equation.

$$u(t) = \sum_{i=1}^{N_I} \sum_{f=1}^{N_i} w_{io} \varepsilon(t - t_i^f) + \rho(t - t^f) \quad (14)$$

where $\varepsilon(s) = (s/\tau) \exp(1 - s/\tau)H(s)$ denotes the spike response function, $\rho(s) = -\theta \exp(-s/\tau_R)H(s)$ indicates the refractoriness function, in which τ and τ_R denote time constant and $H(s)$ signifies the Heaviside function. Like conventional Artificial Neural Network (ANN), SNNs have recurrent, feedforward, and other network frameworks too. In this work, FFNN framework is adopted with output and input layers separated into learning and encoding stages for image classification and recognition.

The presented method is employed for image classification and recognition issues. In coding phase, the latency-phase encoding technique is utilized for transforming the pixels of respective image fields into accurately-timed spike train. Here, the spike train is employed to represent the outside image stimuli data. At the time of learning phase, all the spike trains correspond to input neurons and become the input to SNN. The synaptic weight can be learned using supervised multiple spike learning model. The SNN provides the output for the targeted spike patterns of the provided image.

3 Experimental Validation

The performance validation of the proposed ESFO-EALD technique was conducted using benchmark plant disease dataset [21] and the current section details the same with results. The results were investigated under three test runs. A few sample images are demonstrated in Fig. 3.

The confusion matrix generated by ESFO-EALD technique on test dataset under run-2 is shown in Fig. 4. It is noticed that ESFO-EALD technique categorized 497 images under AS, 488 images under BR, 438 images under CR, and 496 images under HY.

Tab. 1 offers a detailed overview of the results of classification analysis accomplished by ESFO-EALD technique on test run-1. The results demonstrate that ESFO-EALD technique identified the instances under AS class with $acc_y, prec_n, rec_l, spe_y,$ and F_{score} scores such as 0.9923, 0.9842, 0.9861, 0.9944, and 0.9851 respectively. Besides, the outcomes exhibit that the proposed ESFO-EALD method identified the instances under BR class with $acc_y, prec_n, rec_l, spe_y,$ and F_{score} values being 0.9913, 0.9839, 0.9819, 0.9945, and 0.9829 correspondingly. Moreover, ESFO-EALD algorithm recognized the instances under CR class with $acc_y, prec_n, rec_l, spe_y,$ and F_{score} values such as 0.9949, 0.9821, 0.9955, 0.9947, and 0.9887 respectively. Furthermore, the proposed ESFO-EALD approach classified the

instances under HY class with acc_y , $prec_n$, rec_l , spe_y , and F_{score} values being 0.9969, 1.0, 0.988, 1.0, and 0.994.



Figure 3: Sample images

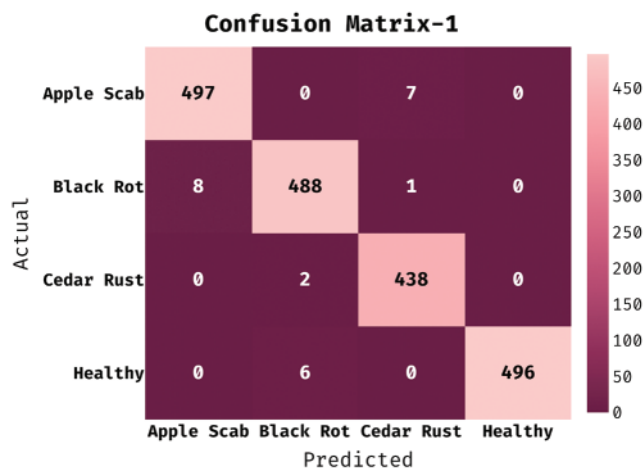
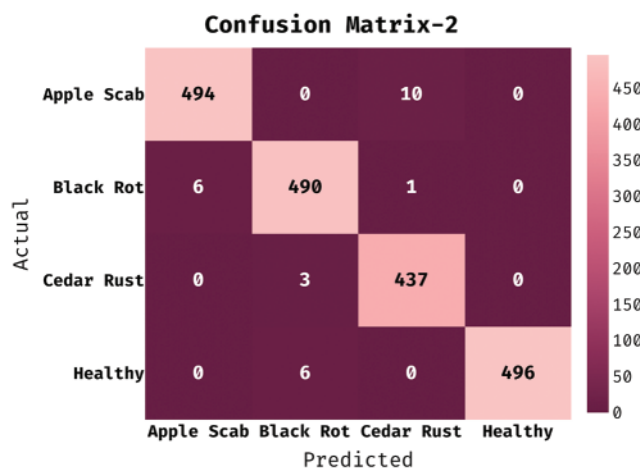


Figure 4: Confusion matrix of ESFO-EALD method on run-1

Table 1: Classification analysis results of ESFO-EALD technique on run-1

Class	acc_y	$prec_n$	rec_l	spe_y	F_{score}
AS	0.9923	0.9842	0.9861	0.9944	0.9851
BR	0.9913	0.9839	0.9819	0.9945	0.9829
CR	0.9949	0.9821	0.9955	0.9947	0.9887
HY	0.9969	1.0	0.988	1.0	0.994
Average	0.9938	0.9875	0.9879	0.9959	0.9877

The confusion matrix generated by ESFO-EALD system on test dataset under run-2 is depicted in Fig. 5. It is clear that the proposed ESFO-EALD approach categorized 494 images under AS, 490 images under BR, 437 images under CR, and 496 images under HY.

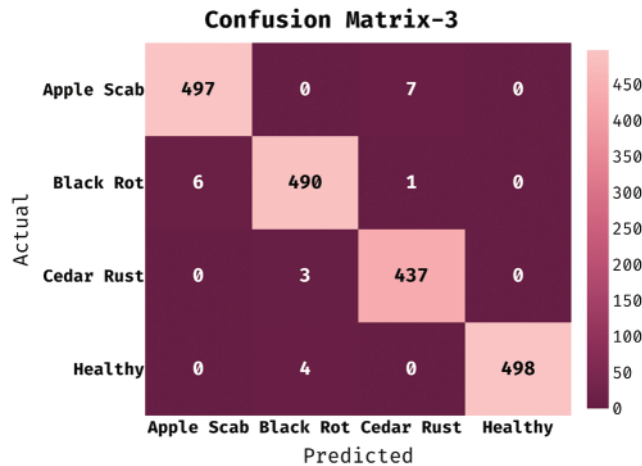
**Figure 5:** Confusion matrix of ESFO-EALD method on run-3

Tab. 2 portrays the results of classification analysis attained by ESFO-EALD method on test run-2. The outcomes portray that ESFO-EALD method categorized the instances under AS class with acc_y , $prec_n$, rec_l , spe_y , and F_{score} values being 0.9918, 0.988, 0.9802, 0.9958, and 0.9841 respectively. Followed by, the outcomes display that the proposed ESFO-EALD algorithm classified the instances under BR class with acc_y , $prec_n$, rec_l , spe_y , and F_{score} values such as 0.9918, 0.982, 0.9859, 0.9938, and 0.9839 correspondingly. Additionally, the results demonstrate that the proposed ESFO-EALD system categorized the instances under CR class by achieving acc_y , $prec_n$, rec_l , spe_y , and F_{score} values such as 0.9928, 0.9754, 0.9932, 0.9927, and 0.9842 respectively. Also, the results showcase that the proposed ESFO-EALD method classified the instances under HY class with acc_y , $prec_n$, rec_l , spe_y , and F_{score} values being 0.9969, 1.0, 0.988, 1.0, and 0.994 correspondingly.

Table 2: Classification analysis results of ESFO-EALD technique on run-2

Class	acc_y	$prec_n$	rec_l	spe_y	F_{score}
AS	0.9918	0.988	0.9802	0.9958	0.9841
BR	0.9918	0.982	0.9859	0.9938	0.9839
CR	0.9928	0.9754	0.9932	0.9927	0.9842
HY	0.9969	1.0	0.988	1.0000	0.994
Average	0.9933	0.9864	0.9868	0.9956	0.9866

The confusion matrix generated by the proposed ESFO-EALD approach on test dataset under run-3 is depicted in Fig. 6. It is observed that ESFO-EALD system categorized 497 images under AS, 490 images under BR, 437 images under CR, and 498 images under HY.

**Figure 6:** Confusion matrix of ESFO-EALD method on run-3

Tab. 3 provides a brief overview of results from classification analysis accomplished by ESFO-EALD method on test run-3. The outcomes show that ESFO-EALD algorithm categorized the instances under AS class with acc_y , $prec_n$, rec_l , spe_y , and F_{score} scores such as 0.9933, 0.9881, 0.9861, 0.9958, and 0.9871 respectively. At the same time, the results demonstrate that ESFO-EALD manner classified the instances under BR class with acc_y , $prec_n$, rec_l , spe_y , and F_{score} values such as 0.9928, 0.9859, 0.9859, 0.9952, and 0.9859 correspondingly. Likewise, the results demonstrate that ESFO-EALD approach placed the instances under CR class with acc_y , $prec_n$, rec_l , spe_y , and F_{score} values such as 0.9943, 0.982, 0.9932, 0.9947, and 0.9876 correspondingly. Eventually, the results demonstrate that ESFO-EALD method identified the instances under HY class with acc_y , $prec_n$, rec_l , spe_y , and F_{score} values such as 0.9979, 1.0, 0.992, 1.0, and 0.996 respectively.

Table 3: Classification analysis results of ESFO-EALD technique on run-3

Class	acc_y	$prec_n$	rec_l	spe_y	F_{score}
AS	0.9933	0.9881	0.9861	0.9958	0.9871
BR	0.9928	0.9859	0.9859	0.9952	0.9859
CR	0.9943	0.982	0.9932	0.9947	0.9876
HY	0.9979	1.0	0.992	1.0000	0.996
Average	0.9946	0.989	0.9893	0.9964	0.9891

Fig. 7 shows the results of accuracy analysis achieved by ESFO-EALD technique under different number of epochs. The figure exposes that the proposed ESFO-EALD system improved both training and validation accuracies with increase in the number of epochs.

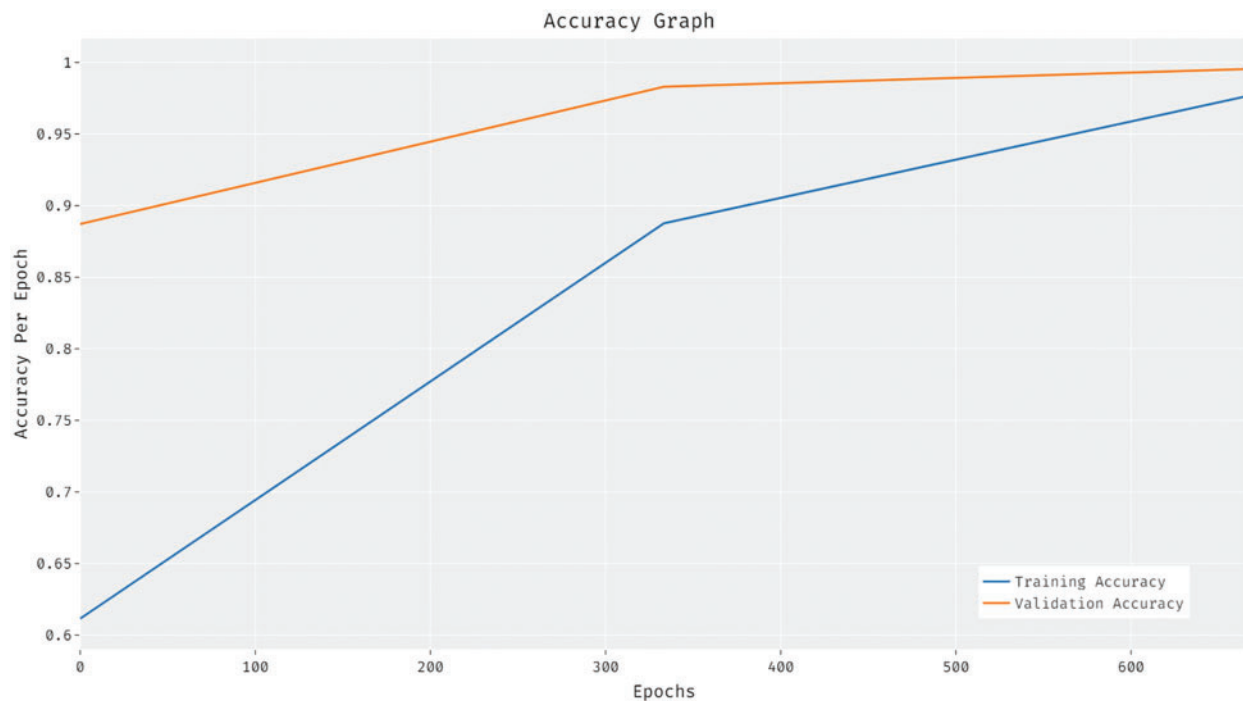
**Figure 7:** Accuracy graph analysis results of ESFO-EALD technique

Fig. 8 portrays the loss analysis results accomplished by ESFO-EALD manner under distinct number of epochs. The figure reveals that ESFO-EALD method gained low training and validation accuracies with increasing number of epochs. Tab. 4 demonstrates the results accomplished by ESFO-EALD algorithm in memory space and training time analysis.

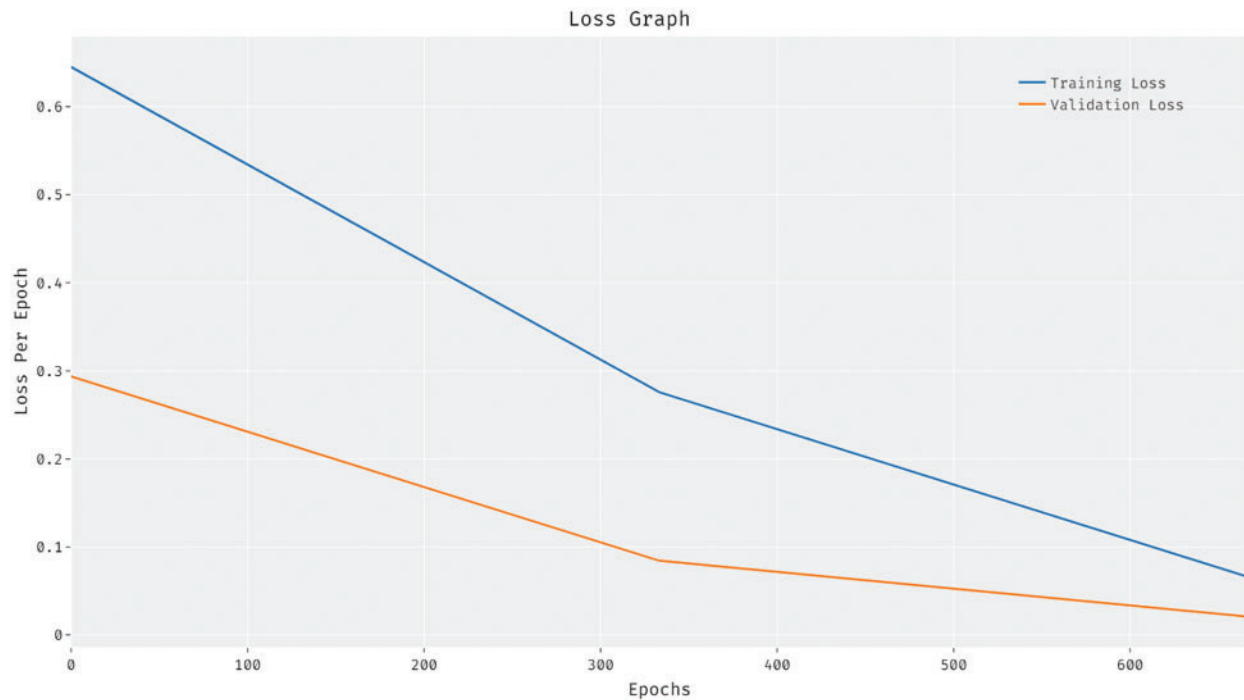


Figure 8: Loss graph analysis of ESFO-EALD technique

Table 4: Comparative analysis results of ESFO-EALD approach in terms of memory space and training time

Methods	Space (MB)	Time (min)
AlexNet	3368.96	33.06
GoogLeNet	4433.92	34.80
VGGNet-16	8908.80	145.98
ResNet-20	12288.00	163.02
DCNN	2897.92	34.74
AIE-ALDC	2621.44	31.08
ESFO-EALD	2138.21	28.65

Fig. 9 demonstrates the results achieved by ESFO-EALD system against other methods in terms of memory space analysis. The results show that visual geometry group (VGGNet)-16 and ResNet-16 models accomplished heavy memory spaces such as 8908.80 and 12288.00 MB respectively. In line with these, both AlexNet and GoogleNet approaches obtained somewhat reduced memory space of 3368.96 and 4433.92 MB respectively. Moreover, DCNN and AI-enabled Apple Leaf Disease Classification (AIE-ALDC) techniques gained considerable memory spaces such as 2897.92 and 2621.44 MB respectively. However, the presented ESFO-EALD technique gained the least memory space of 2138.21 MB.

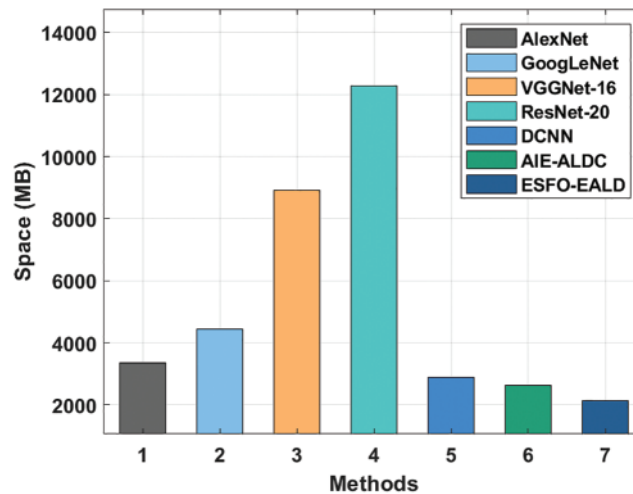


Figure 9: Memory space analysis results of ESFO-EALD approach

Fig. 10 shows the results of training time analysis accomplished by ESFO-EALD method against other systems. The outcomes depict that both VGGNet-16 and ResNet-16 approaches took lengthy training times such as 145.98 and 163.02 min correspondingly. Also, GoogleNet and DCNN systems obtained somewhat reduced training times such as 34.80 and 34.74 min correspondingly. Afterward, AlexNet and AIE-ALDC methods took considerable training times such as 33.06 and 31.08 min correspondingly. However, the presented ESFO-EALD technique consumed a minimum training time of 28.65 min.

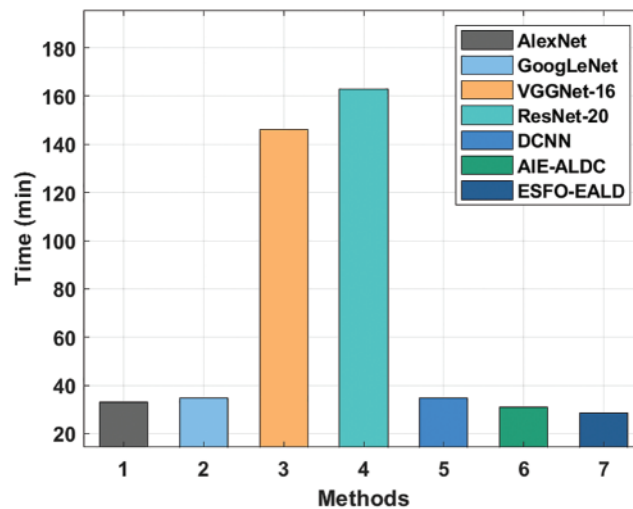


Figure 10: Training time analysis results of ESFO-EALD method

Finally, a detailed comparative *acc*_v analysis was conducted between ESFO-EALD technique and other recent techniques and the results are shown in Tab. 5 and Fig. 11 [22]. The results show that both RNet-101 and RNet-50 models obtained the least *acc*_v values namely, 91.16% and 92.43%. At the same time, slightly improved *acc*_v values such as 93.17% and 93.64% were obtained by RNet-34 and RNet-18 models. Moreover, the improved CNN (ICNN) and AIE-ALDC techniques accomplished reasonable

acc_y values such as 97.14% and 99.20% respectively. However, the proposed ESFO-EALD technique surpassed all other techniques and achieved a maximum acc_y of 99.39%. The above mentioned tables and figures establish that ESFO-EALD technique is an excellent performer in both detection and classification of apple plant leaf images.

Table 5: Comparative analysis results of ESFO-EALD method in terms of accuracy

Methods	Acc_y (%)
RNet-101 model	91.16
RNet-50 model	92.43
RNet-34 model	93.17
RNet-18 model	93.64
ICNN	97.14
AIE-ALDC	99.20
ESFO-EALD	99.39

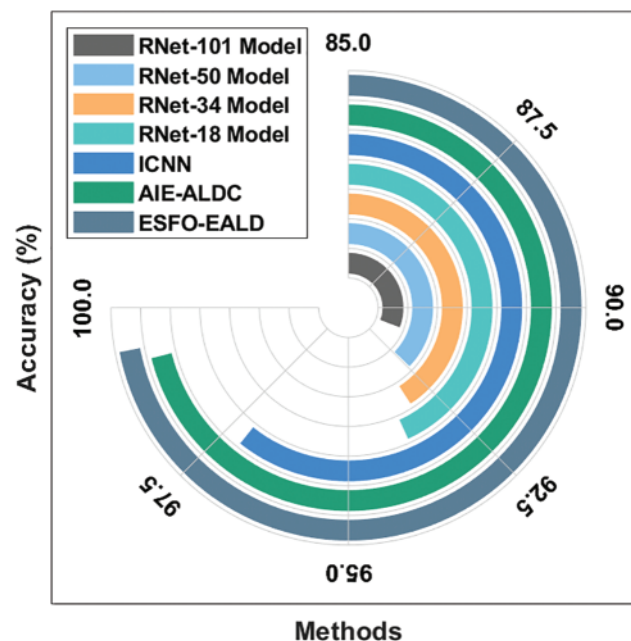


Figure 11: Comparative analysis results of ESFO-EALD method in terms of accuracy

4 Conclusion

In this study, an effective ESFO-EALD technique is developed for identification and classification of apple plant leaf images. The proposed ESFO-EALD approach includes MF-based preprocessing, ESFO with Kapur's entropy-based segmentation, EfficientNet-based Feature extraction, Adam optimizer-based hyperparameter tuning, and SNN-based classification. The utilization of SFO-based threshold value selection and Adam optimizer-based hyperparameter selection helps in accomplishing enhanced outcomes. A wide range of simulations was conducted to validate the effective outcomes

of ESFO-EALD technique on benchmark dataset. The results showcased the betterment of ESFO-EALD technique over recent state-of-the-art approaches. So, it can be concluded that ESFO-EALD technique can be utilized as a proficient tool in detection of plant diseases. In future, the detection performance can be boosted using advanced DL approaches.

Funding Statement: The authors extend their appreciation to the Deanship of Scientific Research at King Khalid University for funding this work under grant number (RGP 2/209/42).

Princess Nourah bint Abdulrahman University Researchers Supporting Project number (PNURSP2022R191), Princess Nourah bint Abdulrahman University, Riyadh, Saudi Arabia.

Conflicts of Interest: The authors declare that they have no conflicts of interest to report regarding the present study.

References

- [1] F. Tongke, "Research on crop leaf disease identification method based on LM-BP neural network," *E3S Web of Conferences*, vol. 131, no. 2, pp. 1118, 2019.
- [2] M. Dutot, L. M. Nelson and R. C. Tyson, "Predicting the spread of postharvest disease in stored fruit, with application to apples," *Postharvest Biology and Technology*, vol. 85, pp. 45–56, 2013.
- [3] A. K. Mahlein, T. Rumpf, P. Welke, H. W. Dehne, L. Plümer *et al.*, "Development of spectral indices for detecting and identifying plant diseases," *Remote Sensing of Environment*, vol. 128, pp. 21–30, 2013.
- [4] L. Yuan, Y. Huang, R. W. Loraamm, C. Nie, J. Wang *et al.*, "Spectral analysis of winter wheat leaves for detection and differentiation of diseases and insects," *Field Crops Research*, vol. 156, pp. 199–207, 2014.
- [5] F. Qin, D. Liu, B. Sun, L. Ruan, Z. Ma *et al.*, "Identification of alfalfa leaf diseases using image recognition technology," *PLOS ONE*, vol. 11, no. 12, pp. e0168274, 2016.
- [6] J. Ma, K. Du, F. Zheng, L. Zhang, Z. Gong *et al.*, "A recognition method for cucumber diseases using leaf symptom images based on deep convolutional neural network," *Computers and Electronics in Agriculture*, vol. 154, pp. 18–24, 2018.
- [7] S. D. Khirade and A. B. Patil, "Plant disease detection using image processing," in *2015 International Conference on Computing Communication Control and Automation*, Pune, India, pp. 768–771, 2015.
- [8] D. A. Bashish, M. Braik and S. B. Ahmad, "Detection and classification of leaf diseases using K-means-based segmentation and neural-networks-based classification," *Information Technology Journal*, vol. 10, no. 2, pp. 267–275, 2011.
- [9] Y. Zhong and M. Zhao, "Research on deep learning in apple leaf disease recognition," *Computers and Electronics in Agriculture*, vol. 168, pp. 105146, 2020.
- [10] K. Michalak and H. Kwasnicka, "Correlation based feature selection method," *International Journal of Bio-Inspired Computation*, vol. 2, no. 5, pp. 319, 2010.
- [11] P. Jiang, Y. Chen, B. Liu, D. He and C. Liang, "Real-time detection of apple leaf diseases using deep learning approach based on improved convolutional neural networks," *IEEE Access*, vol. 7, pp. 59069–59080, 2019.
- [12] B. Liu, Y. Zhang, D. He and Y. Li, "Identification of apple leaf diseases based on deep convolutional neural networks," *Symmetry*, vol. 10, no. 1, pp. 11, 2017.
- [13] A. Umamageswari, N. Bharathiraja and D. S. Irene, "A novel fuzzy c-means based chameleon swarm algorithm for segmentation and progressive neural architecture search for plant disease classification," *ICT Express*, pp. S2405959521001090, 2021.
- [14] M. B. Tahir, M. A. Khan, K. Javed, S. Kadry, Y. D. Zhang *et al.*, "Recognition of apple leaf diseases using deep learning and variances-controlled features reduction," *Microprocessors and Microsystems*, pp. 104027, 2021.
- [15] V. Tiwari, R. C. Joshi and M. K. Dutta, "Dense convolutional neural networks based multiclass plant disease detection and classification using leaf images," *Ecological Informatics*, vol. 63, pp. 101289, 2021.

- [16] E. H. Houssein, M. M. Emam and A. A. Ali, "An efficient multilevel thresholding segmentation method for thermography breast cancer imaging based on improved chimp optimization algorithm," *Expert Systems with Applications*, vol. 185, pp. 115651, 2021.
- [17] M. Li, Y. Li, Y. Chen and Y. Xu, "Batch recommendation of experts to questions in community-based question-answering with a sailfish optimizer," *Expert Systems with Applications*, vol. 169, pp. 114484, 2021.
- [18] X. Cui, D. Wang and Z. J. Wang, "Multi-scale interpretation model for convolutional neural networks: Building trust based on hierarchical interpretation," *IEEE Transactions on Multimedia*, vol. 21, no. 9, pp. 2263–2276, 2019.
- [19] X. Jiang, B. Hu, S. C. Satapathy, S. H. Wang and Y. D. Zhang, "Fingerspelling identification for chinese sign language via alexnet-based transfer learning and adam optimizer," *Scientific Programming*, vol. 2020, no. 3, pp. 1–13, 2020.
- [20] D. Liu and S. Yue, "Video-based disguise face recognition based on deep spiking neural network," in *2018 International Joint Conference on Neural Networks (IJCNN)*, Rio de Janeiro, pp. 1–8, 2018.
- [21] <https://www.kaggle.com/vipooooool/new-plant-diseases-dataset/data#>.
- [22] F. N. A. Wesabi, A. A. Albraikan, A. M. Hilal, M. M. Eltahir, M. A. Hamza *et al.*, "Artificial intelligence enabled apple leaf disease classification for precision agriculture," *Computers, Materials & Continua*, vol. 70, no. 3, pp. 6223–6238, 2022.